# Control of a Grid-connected Inverter using Sliding Mode Control

**Quang-Tho Tran**
Faculty of Electrical and Electronics Engineering, HCMC University of Technology and Education, Vietnam
thotq@hcmute.edu.vn (corresponding author)

*Received: 24 March 2024 | Revised: 16 April 2024 | Accepted: 24 April 2024*



**ABSTRACT**

**The rising popularity of grid-connected multilevel inverters with photovoltaic panels underscores the importance of effective modulation and control strategies for ensuring optimal power quality. The performance of these inverters hinges significantly on modulation and control approaches, specifically addressing issues like common mode voltage, harmonics, switching loss, and dynamic response. This study introduces a novel approach to mitigate current harmonics in these inverters by employing sliding mode control. Notably, this technique achieves harmonic reduction without necessitating an increase in the switching count. The presented technique eliminates phase-locked loop, current controllers, and carrier waves, thereby easing hardware computation. Beyond computational efficiency, this approach contributes to enhanced power quality and dynamic response within the inverter system. Simulation results affirm the efficacy of the proposed method when compared to the use of the phase opposite disposition modulation combined with the current controllers. In the nominal operational mode, the proposed method reduces the current Total Harmonic Distortion (THD), the highest magnitude of individual harmonics, and the switching count by 43.6%, 73.5%, and 19.6% respectively, compared with those of the method using the phase opposite disposition modulation combined with current controllers.**

***Keywords-cascaded multilevel inverter; sliding mode control; switching count; THD; individual harmonic***

## I. INTRODUCTION

The surge in popularity of renewable energies stems from their eco-friendly attributes and growing cost competitiveness. Wind turbines and solar panels are now pivotal in addressing climate change, mitigating pollution, and ensuring long-term energy sustainability, garnering interest across various industries. However, the power of these sources is highly dependent on weather conditions. To serve as efficient power sources, seamless integration into the power grid is crucial, achieved through inverters. Multilevel inverters offer numerous benefits, including reduced Total Harmonic Distortion (THD), increased voltage capacity, and increased efficiency. Collectively, these advantages enhance the overall performance of the system [1-3]. These technologies find applications in renewable energy systems, high-voltage transmission, motor drives, and electric vehicles, effectively addressing complex power conversion needs. Multilevel inverters play an essential role in grid-connected energy systems by efficiently converting direct current from sources like solar panels into grid-compatible alternating current. Their widespread adoption is due to their role in facilitating smooth integration, enhancing energy yields, and advancing sustainable power generation [4-6]. Given that the need for energy-efficient and environmentally friendly solutions rises, their popularity is anticipated to keep expanding [4, 5, 7-10]. The inverter system control includes the controllers at the dc side, current controllers, modulation using carrier waves, and the controller in the Phase-Locked Loop (PLL) to synchronize with the power grid. Thus, the control quality of the inverter system depends on the aforementioned factors. Especially, the substantial Common Mode Voltage (CMV) magnitude has a detrimental impact on the power quality of grid-connected inverter systems, leading to the generation of grid-leakage currents and harmonics [11]. Several methods are available for modulating multilevel inverters, with primary options including Sinusoidal Pulse-Width modulation (SPWM) and space vector modulation [12-15]. Modulating with SPWM is proved to be more efficient than using space vector modulation as the number of levels increases. Various techniques consisting of Phase Disposition (PD), Phase Opposite Disposition (POD), and Alternate Phase Opposite Disposition (APOD) [16-18], have their own advantages and disadvantages. POD and APOD exhibit the ability to produce a CMV with lower magnitude compared to PD. The POD technique is more widely adopted for modulation due to its simplicity and efficiency. However, it requires the use of carrier waves for modulation.

Various controllers regulate the current of grid-connected inverters, including the Proportional-Integrator (PI), Proportional-Resonance (PR), fuzzy logic, neural networks, model predictive control, and Sliding Mode Control (SMC). SMC stands out for variable structure control systems. Renowned for robustness against uncertainties, it maintains stability in dynamic environments. Its rapid convergence to desired states and minimal tracking errors enhance precision. SMC's versatility extends across applications, from mechanical to electronic systems, establishing it as a valuable tool in the modern control theory. The difference between the SMC and other control methods in controlling the grid-connected inverters is the ability to offer better dynamic responses, smaller over-shoot or under-shoot, and lower steady-state error. However, the chattering phenomenon is one of the problems that need to be solved. Although the SMC techniques have also been introduced in [19-23] and adopted for control in motor drives [24-28], they have not been efficiently employed in the field of grid-connected inverters. Authors in [29, 30] used the SMC for controlling the dc side of the single phase inverter. Authors in [31, 32] introduced the 2-level single phase inverters. Authors in [33-37] applied the 2-level 3-phase inverters. Authors in [38] deployed multilevel 3-phase inverter requiring additional sensors of filter capacitor voltages. The technique in [39] was only applied to the inverter, not to the grid-connected inverter. This technique solely improves modulation, while the control of the grid-connected inverter system consists of calculating the reference currents from the reference powers, current control, modulation, and synchronization.

This paper introduces a control technique for grid-connected multilevel three-phase inverters following the SMC method. Notably, this method eliminates the use of carrier waves in modulation, and completely removes the PLL and current controllers from the control system, simplifying hardware calculations. The presented approach enhances power quality and dynamic response. The proposed method does not need to measure the voltage of the filter capacitor. The ability to spread the spectrum also helps significantly reduce the magnitude of individual harmonics.

## II. GRID-CONNECTED INVERTER SYSTEM

In Figure 1, a 5-level 3-phase inverter system connected to the grid is depicted. The system employs POD modulation, reference current calculation, a current controller, and a PLL for control. Deploying the current control method in the Synchronous Rotating Frame (SRF), quantities like $I_d$, $I_q$, $V_d$, and $V_q$ are transformed from the three-phase frame using the phase angle ($\theta$) estimated by the PLL. Subsequently, the reference currents injected into the grid in the SRF, namely $I_{d\text{-ref}}$ and $I_{q\text{-ref}}$, are calculated according to (1) based on reference powers $P_{ref}$ and $Q_{ref}$.

$$\begin{bmatrix} I_{d-ref} \\ I_{q-ref} \end{bmatrix} = \frac{(2/3)}{V_d^2 + V_q^2} \begin{bmatrix} V_d & -V_q \\ V_q & V_d \end{bmatrix} \begin{bmatrix} P_{ref} \\ Q_{ref} \end{bmatrix} \qquad (1)$$

The current controller within the grid-connected inverters has the task of governing the current flow into the grid, ensuring alignment with the designated power reference prerequisites. This controller commonly applies a PI control algorithm, enabling adjustments to the inverter's output voltage for the purpose of sustaining the current at the intended reference level. Based on the error between the reference currents and the actual measurements, these controllers fine-tune the reference voltages, specifically $V_{d\text{-ref}}$ and $V_{q\text{-ref}}$. These voltage values are then transformed into their corresponding reference phase voltages, denoted as $V_{\text{ref-abc}}$. The POD modulation method uses these phase voltages as inputs, generating pulse signals for switches.

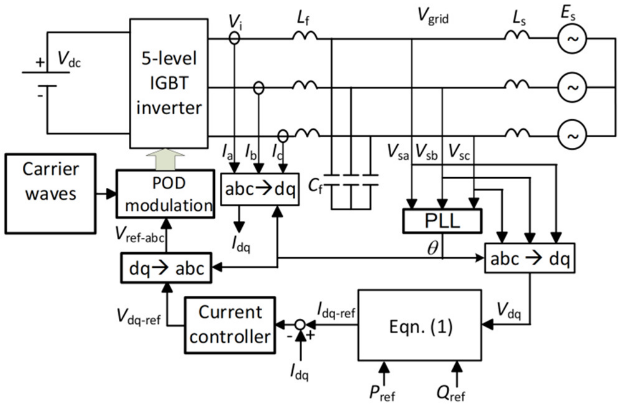


Fig. 1. Structure of the grid-connected multilevel inverter system.

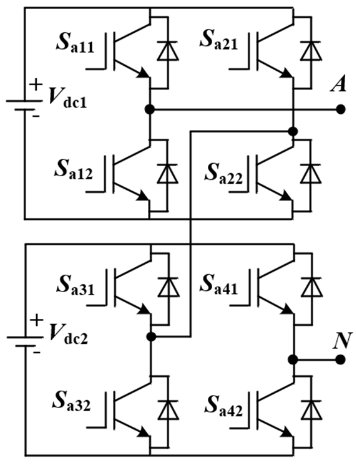

Fig. 2. Main circuit for phase A.

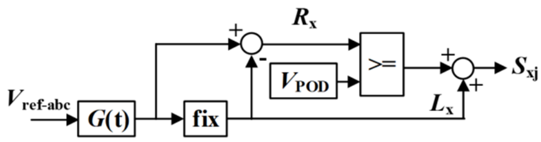


Fig. 3. Control diagram of the inverter.

TABLE I. SWITCHING STATES OF SWITCHES IN PHASE A

| *n* | $S_{a11}$ | $S_{a21}$ | $S_{a31}$ | $S_{a41}$ | Output voltage |
|---|---|---|---|---|---|
| 1 | 0 | 1 | 0 | 1 | -2 $V_{dc}$ |
| 2 | 0 | 1 | 0 | 0 | $-V_{dc}$ |
| 3 | 0 | 0 | 0 | 0 | 0 |
| 4 | 1 | 0 | 0 | 0 | $+V_{dc}$ |
| 5 | 1 | 0 | 1 | 0 | +2 $V_{dc}$ |

$$G(t) = \left(V_{\text{ref-abc}} + 1\right)\frac{n-1}{2} \qquad (2)$$

$$L_x = \begin{cases} n-2 & \text{if } G(t) \geq 2 \\ fix(G(t)), & otherwise \end{cases} \quad (3)$$

The illustration in Figure 2 displays the main circuit for one phase, featuring a pair of H-bridges utilizing IGBT switches. Each arm of this configuration comprises an upper switch, $S_{xj1}$, and a lower switch, $S_{xj2}$ (where $j$ ranges from 1 to 4). The output voltage for each phase is detailed in Table I, encompassing five distinct levels. These voltage levels are contingent upon the outputs $S_{xj}$ as indicated in the control diagram portrayed in Figure 3. Within this control diagram, the voltage $G(t)$ is delineated into two constituents, $R_x$ and $L_x$ (where $x$ represents $a$, $b$, or $c$). The signal $G(t)$ has been normalized according to the inverter levels defined in (2). The integer component, $L_x$ ($0 \leq L_x \leq n-2$), is determined from the signal $G(t)$ in (3). Additionally, $R_x$ (with the constraint $0 \leq R_x \leq 1$) is the result of subtracting $L_x$ from $G(t)$.

## III. THE PROPOSED METHOD

The structure of the proposed method following the SMC technique is shown in Figure 4. The reference currents are calculated based on the grid phase voltages and the reference powers. These phase voltages are transformed as in (4). Then, based on the reference powers $P_{ref}$ and $Q_{ref}$, the reference currents are calculated as in (5) and transformed into the reference phase currents in (6). These currents are employed to input the proposed SMC block in Figure 4. The proposed control diagram using the SMC method is demonstrated in Figure 5(a). The PWM block utilizing a constant C for modulation in Figure 5(a) applies the technique of [40] and does not use carrier waves. The SMC method holds several key advantages in control systems. Despite its advantages, careful design is required to manage chattering phenomena and high-frequency switching, which can affect system behavior and efficiency.

$$\begin{bmatrix} v_\alpha \\ v_\beta \end{bmatrix} = \begin{bmatrix} 2/3 & -1/3 & -1/3 \\ 0 & 1/\sqrt{3} & -1/\sqrt{3} \end{bmatrix} \begin{bmatrix} v_{ag} \\ v_{bg} \\ v_{cg} \end{bmatrix} \quad (4)$$

$$\begin{bmatrix} i_{\alpha ref} \\ i_{\beta ref} \end{bmatrix} = \frac{(2/3)}{V_\alpha^2 + V_\beta^2} \begin{bmatrix} V_\alpha & V_\beta \\ V_\beta & -V_\alpha \end{bmatrix} \begin{bmatrix} P_{ref} \\ Q_{ref} \end{bmatrix} \quad (5)$$

$$\begin{bmatrix} i_{aref} \\ i_{bref} \\ i_{cref} \end{bmatrix} = \begin{bmatrix} 1 & 0 \\ -1/2 & \sqrt{3}/3 \\ -1/2 & -\sqrt{3}/2 \end{bmatrix} \begin{bmatrix} i_{\alpha ref} \\ i_{\beta ref} \end{bmatrix} \quad (6)$$

Based on Figure 4, the output voltage of the inverter can be described as follows:

$$v_i(t) = L_f \frac{di(t)}{dt} + R.i(t) + v_g(t) \quad (7)$$

where $i(t)$ is the output phase current of the inverter, $v_g(t)$ is the phase voltage of the grid source, $L_f$ is the inductor of the filter, and $R$ is the resistor of $L_f$. Equation (7) can also be rewritten as (8), where the dot (˙) above the letter $i$ represents the derivative of the current $i$. A first-order low-pass digital filter in [41] is also used in Figure 5 with the transfer function of (9), where $p$ is a derivative operator and $T$ is a time constant.

$$v_i = L_f \dot{i} + Ri + v_g \quad (8)$$

$$F(p) = \frac{1}{T.p+1} \quad (9)$$

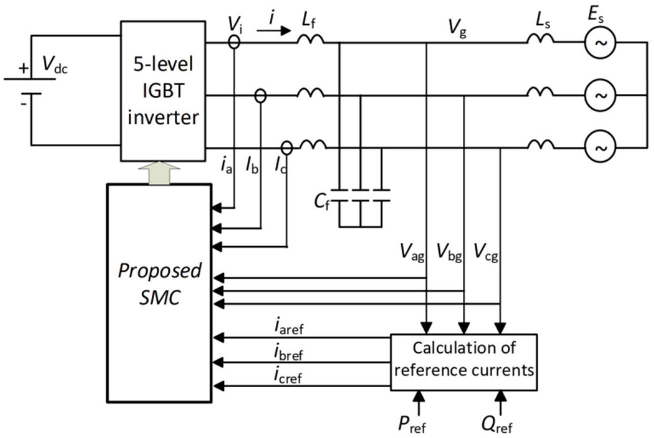


Fig. 4. Proposed method using the SMC technique.

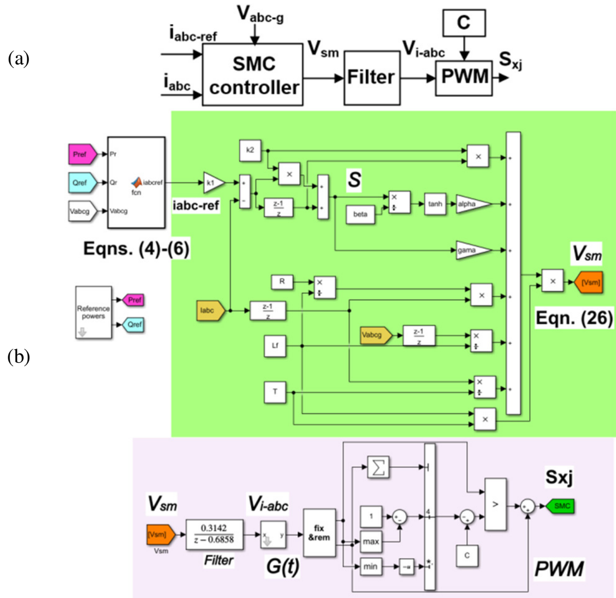


Fig. 5. Proposed control technique using SMC. (a) Principle diagram, (b) detailed diagram in Matlab/Simulink.

The inverter phase voltage $v_i$ in Figure 5 is also defined as (10), where $v_{sm}$ is the output of the sliding mode controller and the input of the filter. Equation (10) can be rewritten as (11). Substituting (8) into (11), the resulting voltage $v_{sm}$ can be seen in (12). Equation (13) can be deuced from (12).

$$v_i = \frac{v_{sm}}{T.p+1} \quad (10)$$

$$T.\dot{v}_i + v_i = v_{sm} \quad (11)$$

$$v_{sm} = L_f \dot{i} + Ri + v_g + T\left(L_f \ddot{i} + R\dot{i} + \dot{v}_g\right) \qquad (12)$$

$$\ddot{i} = \frac{\left[v_{sm} - L_f \dot{i} - Ri - v_g - T\left(R\dot{i} + \dot{v}_g\right)\right]}{TL_f} \qquad (13)$$

The current error between the reference current and the actual one $e$ is defined in (14), where $i_{\text{ref}}$ and $i$ are the reference current and the measured one, respectively, and $k_1$ is a positive constant used for eliminating the steady-state error. The derivative of the current error is written in (15). Providing that (12) is a second-order function, the sliding surface $S$ is chosen as in (16), where $k_2$>0 is a positive constant to satisfy the stable Hurwitz condition. It can also deduce the derivative of the sliding surface as in (17).

$$e = k_1 i_{ref} - i \qquad (14)$$

$$\dot{e} = k_1 \dot{i}_{ref} - \dot{i} \qquad (15)$$

$$S = \dot{e} + k_2 e \qquad (16)$$

$$\dot{S} = \ddot{e} + k_2 \dot{e} \qquad (17)$$

From (15) and (17), the derivative of the sliding surface of (18) can be deduced. Substituting (13) into (18), the result of (19) is obtained. The control law is chosen as (20) to approach the sliding surface, where $\alpha$, $\beta$, and $\gamma$ are positive constants. The hyperbolic tangent is usually chosen to reduce the chattering phenomena. According to the Lyapunov theory, a positive definite function $L$ and its derivative are seen in (21) and (22).

$$\dot{S} = k_1 \ddot{i}_{ref} - \ddot{i} + k_2 \dot{e} \qquad (18)$$

$$\dot{S} = k_1 \ddot{i}_{ref} - \frac{\left[v_{sm} - L_f \dot{i} - Ri - v_g - T\left(R\dot{i} + \dot{v}_g\right)\right]}{TL_f} + k_2 \dot{e} \qquad (19)$$

$$\dot{S} = -\alpha.\tan sig\left(\frac{S}{\beta}\right) - \gamma S + \frac{Ri + v_g}{TL_f} + k_1 \ddot{i}_{ref} \qquad (20)$$

$$L = \frac{S^2}{2} \qquad (21)$$

$$\dot{L} = S\dot{S} \qquad (22)$$

Thus:

$$S\dot{S} = S\left[-\alpha.\tan sig\left(\frac{S}{\beta}\right) - \gamma S + \frac{Ri + v_g}{TL_f} + k_1 \ddot{i}_{ref}\right] \qquad (23)$$

with:

$$\alpha > \left|\frac{Ri + v_g}{TL_f} + k_1 \ddot{i}_{ref}\right| \qquad (24)$$

When the condition of (24) is satisfied, it can infer as (25). Equation (25) is always true with a large value of $\gamma$. According to the Lyapunov theory, the system is stable. Therefore, from (19) and (20), the input voltage of the filter can be obtained as (26).

$$S\dot{S} = -\alpha\left|\frac{S}{\beta}\right| - \gamma S^2 - S\left(\frac{Ri + v_g}{TL_f} + k_1 \ddot{i}_{ref}\right) < -\alpha\left|\frac{S}{\beta}\right| < 0 \qquad (25)$$

$$v_{sm} = TL_f\left[\alpha \tan sig\left(\frac{S}{\beta}\right) + \gamma S + k_2 \dot{e} + \frac{R\dot{i} + \dot{v}_g}{L_f} + \frac{\dot{i}}{T}\right] \qquad (26)$$

The SMC technique in Matlab/Simulink is shown in detail in Figure 5(b).

## IV. RESULTS AND DISCUSSION

The system parameters are presented in Table II. There are three intervals of time surveyed in this system. The time of each interval is 0.2 s. In the first interval, 0-0.2 s, the reference active power $P_{\text{ref}}$ is 20 kW, the reference reactive power $Q_{\text{ref}}$ is 0.0 Var. In the second interval, 0.2-0.4 s, $P_{\text{ref}}$ is stepped down to 10 kW whilst $Q_{\text{ref}}$ is still 0.0 Var. In the third interval, 0.4-0.6 s, $P_{\text{ref}}$ is still 10 kW whereas $Q_{\text{ref}}$ is stepped from 0.0 Var to 10 kVar.

TABLE II. SYSTEM PARAMETERS

| Parameter | Symbol | Value |
|---|---|---|
| Grid source voltage | $V_g$ | 3*380 VAC |
| Grid source frequency | $f_m$ | 50 Hz |
| Resistor of the grid source | $R_s$ | 0.01 Ω |
| Inductor of the grid source | $L_s$ | 0.1 mH |
| Inductor of filter | $L_f$ | 2.5 mH |
| Resistor of $L_f$ | $R$ | 0.01 Ω |
| Capacitor of filter | $C_f$ | 1 mF |
| DC voltage | $V_{dc}$ | 170 V |
| Coefficients of current controller | $K_p$; $K_i$ | 0.15; 20 |
| Frequency of carrier wave in POD | $f_{car}$ | 2.5 kHz |
| Constants | $k_1$; $k_2$; $C$ | 1.05; 3.1; 0.5 |
| | $\alpha$; $\beta$; $\gamma$ | 700; 1.1; 4.08*$10^5$ |
| Time constant of the filter | $T$ | 3.96*$10^{-5}$ |

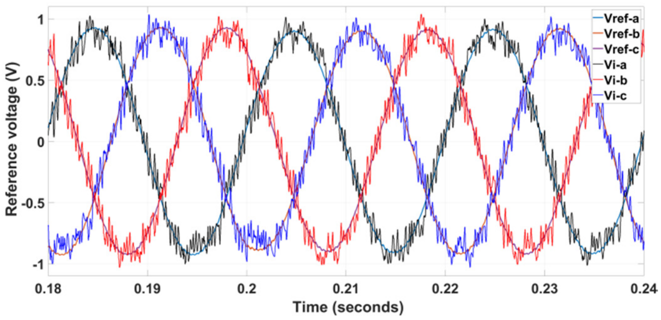


Fig. 6. Waveforms of the reference phase voltages from 0.18-0.24 s: $v_{\text{ref-a}}$; $v_{\text{ref-b}}$; $v_{\text{ref-c}}$ of the POD method and $v_{\text{i-a}}$; $v_{\text{i-b}}$; $v_{\text{i-c}}$ of the proposed method.

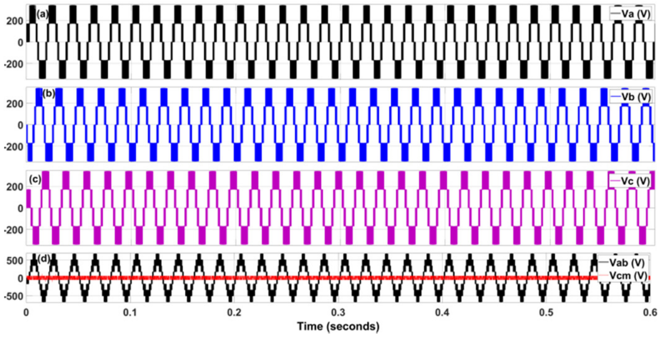


Fig. 7. Voltage waveforms of the PI-POD method taken at the inverter output and before the LC filter. (a)-(c) Phase voltages, (d) line-line voltage and common mode voltage.

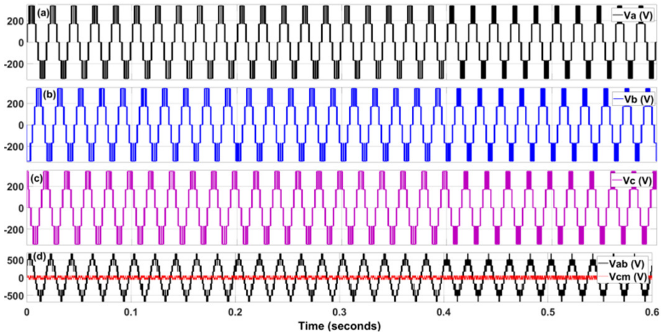


Fig. 8. Voltage waveforms of the SMC method taken at the inverter output and before the LC filter. (a)-(c) Phase voltages, (d) line-line voltage and common mode voltage.

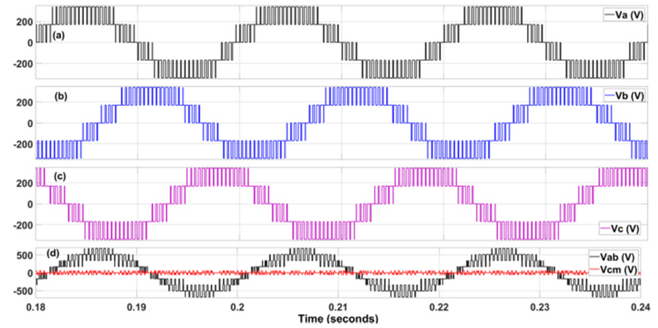


Fig. 9. Voltage waveforms zoomed during 0.18-0.24 s of the PI-POD method. (a)-(c) Phase voltages, (d) line-line and common mode voltages.

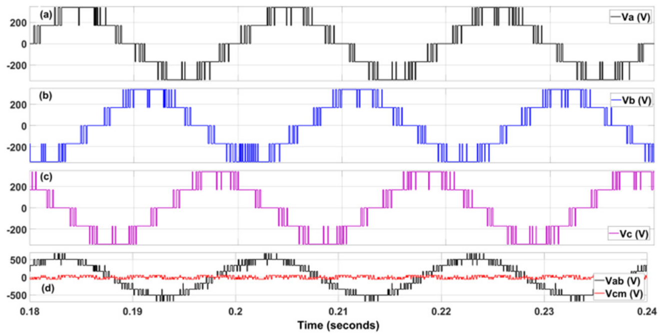


Fig. 10. Voltage waveforms zoomed in 0.18-0.24 s of the SMC method. (a)-(c) Phase voltages, (d) line-line voltage and common mode voltage.

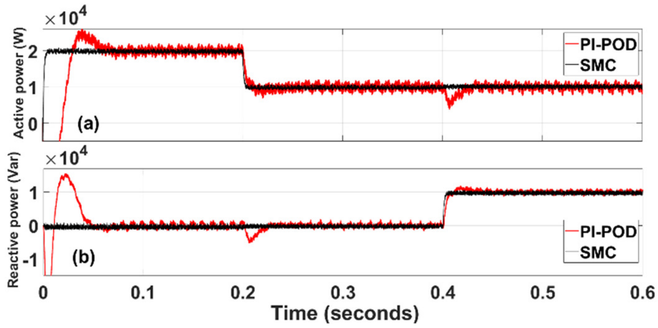


Fig. 11. Powers injected into the grid: (a) Active power, (b) reactive powers.

The surveyed results are displayed in Figures 6-15. The waveforms of the reference phase voltages in Figure 6 revealed a significant difference between the signals of the PI-POD method and the proposed one using SMC. The signals $v_{refa}$, $v_{refb}$, and $v_{refc}$ are the reference voltages of the PI-POD method used to modulate the inverter. They are also the signals $v_{ref\text{-}abc}$ in Figure 3 and (2). These signals are relatively smooth compared to the waveforms $v_{ia}$, $v_{ib}$, and $v_{ic}$ ($v_i$ in Figure 4 or $v_{i\text{-}abc}$ in Figure 5) of the proposed method. The ripples of the waveform $v_{i\text{-}abc}$ also improve the dynamics. The waveforms of phase voltages, line-line voltage, and CMV of the two methods are illustrated in Figures 7-8. These voltage waveforms are taken at the output of the inverter and before the LC filter in Figure 1. They are also zoomed in Figures 9-10 from 0.18 s to 0.24 s.

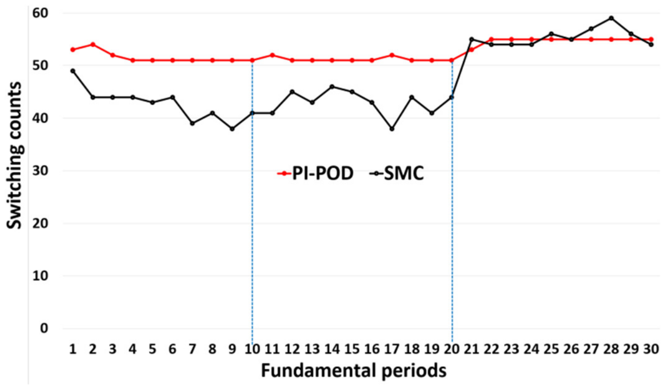


Fig. 12. Switching count in each half of fundamental period of the two methods.

The magnitude of CMV in Figure 10(d) of the SMC is $V_{dc}/3$, also equivalent to that of the POD method in Figure 9(d). This indicates that the proposed SMC offers a reduced CMV like that of the POD method. Moreover, the zoomed waveforms of the two methods in Figures 9-10 exhibited that the number of switching counts of the proposed method is significantly lower than that of the PI-POD method. In the entire surveyed time, there are 30 fundamental periods. In the first two intervals, of 20 periods, the system only generates active power into the grid. This is the operational mode usually used in grid-connected inverters and shown in Figure 11. The switching count of the proposed method in the two first intervals in Figure 12 is always lower than 46, whereas that of the PI-POD method is always higher than 51. In the third interval, of 21-30 fundamental periods, and with generation of reactive power into the grid, the switching count of the proposed method is similar to that of the PI-POD method. Although the switching count of the proposed method is always equal or lower than that of the PI-POD method, the ripples of the phase currents generated into the grid of the proposed method in Figure 13(b) are smaller than those of the PI-POD method in Figure 13(a). This is demonstrated more clearly when the current waveforms are zoomed from 0.18 to 0.24 s in Figure 14. The ability to reduce the voltage harmonics of the SMC method helps the 3-phase current waveforms generated into the grid in Figure 14 to be smoother than those of the PI-POD method.

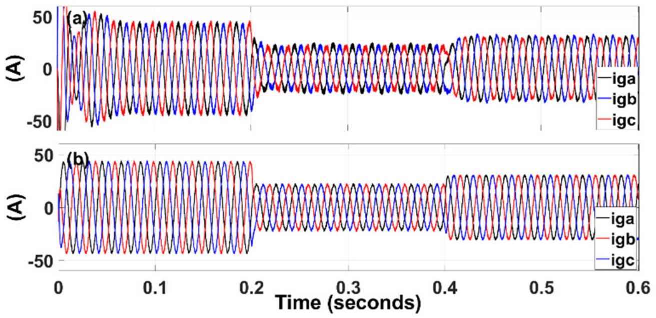


Fig. 13. Current waveforms generated into the grid: (a) PI-POD, (b) SMC.

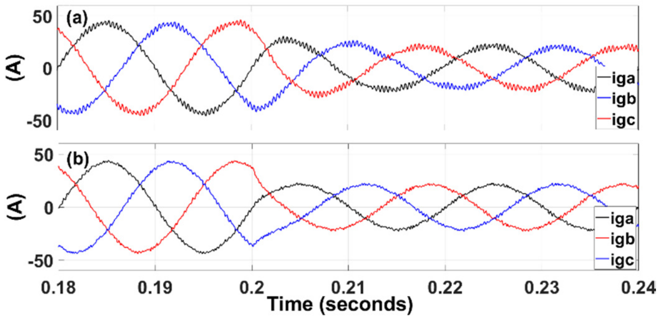


Fig. 14. Current waveforms generated into the grid zoomed in 0.18-0.24 s: (a) PI-POD, (b) SMC.

The phase current THD value of the proposed method in Figure 15 is significantly smaller than that of the PI-POD method. The spectra and phase current THD for phase A of the two methods are also manifested in Figure 15. The current THD values are taken in the last period of each time interval at the moments 0.18 s, 0.38 s, and 0.58 s. The THD values of the PI-POD method in Figures 15(a)-(c) are 4.61%, 9.5%, and 5.62%, respectively. These values are always higher than those of the SMC method in Figures 15(d)-(f), which are 2.6%, 4.87%, and 3.47, respectively. In addition, the highest magnitudes of the individual harmonics in Figures 15(a)-(c) of the PI-POD method are up to 2.8%, 5.58%, and 3.32%, correspondingly. On the contrary, those in Figures 15(d)-(f) of the SMC method are only 0.74%, 1.07%, and 0.94%, accordingly. Thus, in the first interval, i.e. during the nominal operational mode, the reduction of current THD of the proposed method is 43.6% that of the PI-POD method. Similarly, the highest magnitude of the individual current harmonic reduces by 73.5%. The switching count is 41, lower than the 51 of the PI-POD (Figure 12), being reduced by 19.6%.

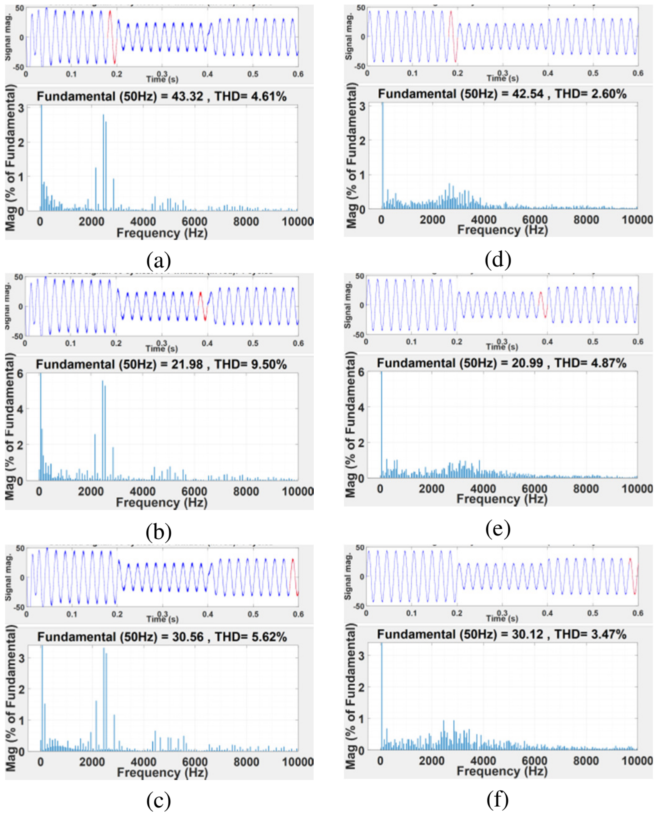


Fig. 15. Spectra and THD of phase current A. (a)-(c) PI-POD method, (d)-(f) proposed SMC method.

Due to the lower ripples of the phase current, the power ripples of the proposed SMC method are also smaller than those of the PI-POD method (Figure 11). Moreover, the power dynamic response of the SMC method is also better while that of the PI-POD method takes over 2 fundamental periods. The power dynamic response of the SMC method is better because there are no current controllers, PLL, and carrier waves. Furthermore, the over-shoot or under-shoot of powers of the proposed method are also lower those that of the PI-POD method.

## V. CONCLUSION

This paper presented the effects of controllers and modulation on the dynamic response and power quality of grid-connected inverters. The proposed method utilizes the SMC for the control and modulation of the grid-connected inverters. The design of the sliding surface is based on the first-order low-pass filter and deploys the function of hyperbolic tangent for eliminating the chattering phenomenon. In the proposed SMC technique, the phase-locked-loop, current controllers, and carrier waves are completely removed from the inverter control system. This reduces the computations to the hardware and improves the dynamic response. The proposed method does not need to measure the voltage of the filter capacitor. The ability to spread the spectrum also significantly reduces the magnitude of the individual harmonics.

The simulation results based on the grid-connected system employing a cascaded 5-level 3-phase inverter confirmed the effectiveness of the proposed method compared to that of the method using the POD modulation combined with current controllers. The dynamic response, overshoot/undershoot, CMV, THD values, individual harmonics, and the number of switching counts were considered and evaluated quantitatively. In the nominal operational mode, the proposed method reduces the current THD, the highest magnitude of the individual harmonic, and the switching count by 43.6%, 73.5%, and 19.6% respectively, in comparison with those of the PI-POD method.

## ACKNOWLEDGMENT

This work belongs to the project in 2024 funded by Ho Chi Minh City University of Technology and Education, Vietnam.

## REFERENCES

[1] U. B. Tayab and M. A. A. Humayun, "Modeling and Analysis of a Cascaded Battery-Boost Multilevel Inverter Using Different Switching Angle Arrangement Techniques," *Engineering, Technology & Applied Science Research*, vol. 7, no. 2, pp. 1450–1454, Apr. 2017, https://doi.org/10.48084/etasr.1094.

[2] Y. Gopal, K. P. Panda, D. Birla, and M. Lalwani, "Swarm Optimization-Based Modified Selective Harmonic Elimination PWM Technique Application in Symmetrical H-Bridge Type Multilevel Inverters," *Engineering, Technology & Applied Science Research*, vol. 9, no. 1, pp. 3836–3845, Feb. 2019, https://doi.org/10.48084/etasr.2397.

[3] K. Gudipati, H. V. R. Maramreddy, S. G. Kolli, V. A. Lakshmi, and G. S. Reddy, "Comparison of Pulse Width Modulation Techniques for Diode-Clamped and Cascaded Multilevel Inverters," *Engineering, Technology & Applied Science Research*, vol. 13, no. 4, pp. 11078–11084, Aug. 2023, https://doi.org/10.48084/etasr.5939.

[4] S. Mehta and V. Puri, "A review of different multi-level inverter topologies for grid integration of solar photovoltaic system," *Renewable Energy Focus*, vol. 43, pp. 263–276, Dec. 2022, https://doi.org/10.1016/j.ref.2022.10.002.

[5] G. Griva, S. Musumeci, R. Bojoi, P. Zito, S. Bifaretti, and A. Lampasi, "Cascaded multilevel inverter for vertical stabilization and radial control power supplies," *Fusion Engineering and Design*, vol. 189, Apr. 2023, Art. no. 113473, https://doi.org/10.1016/j.fusengdes.2023.113473.

[6] A. Mittal, K. Janardhan, and A. Ojha, "Multilevel inverter based Grid Connected Solar Photovoltaic System with Power Flow Control," in *International Conference on Sustainable Energy and Future Electric Transportation*, Hyderabad, India, Jan. 2021, pp. 1–6, https://doi.org/10.1109/SeFet48154.2021.9375753.

[7] W. Rahmouni, G. Bachir, and M. Aillerie, "A new control strategy for harmonic reduction in photovoltaic inverters inspired by the autonomous nervous system," *Journal of Electrical Engineering*, vol. 73, no. 5, pp. 310–317, Sep. 2022, https://doi.org/10.2478/jee-2022-0041.

[8] N. T. Mbungu, R. M. Naidoo, R. C. Bansal, M. W. Siti, and D. H. Tungadio, "An overview of renewable energy resources and grid integration for commercial building applications," *Journal of Energy Storage*, vol. 29, Jun. 2020, Art. no. 101385, https://doi.org/10.1016/j.est.2020.101385.

[9] J. Stöttner, A. Rauscher, and C. Endisch, "Pareto optimization of multilevel inverter structures regarding the DC magnitude, switching frequency and switching angles," *International Journal of Electrical Power & Energy Systems*, vol. 142, no. Part A, Nov. 2022, Art. no. 108259, https://doi.org/10.1016/j.ijepes.2022.108259.

[10] C. Dhanamjayulu, P. Sanjeevikumar, and S. M. Muyeen, "A structural overview on transformer and transformer-less multi level inverters for renewable energy applications," *Energy Reports*, vol. 8, pp. 10299–10333, Nov. 2022, https://doi.org/10.1016/j.egyr.2022.07.166.

[11] C.-C. Hou, C.-C. Shih, P.-T. Cheng, and A. M. Hava, "Common-Mode Voltage Reduction Pulsewidth Modulation Techniques for Three-Phase Grid-Connected Converters," *IEEE Transactions on Power Electronics*, vol. 28, no. 4, pp. 1971–1979, Apr. 2013, https://doi.org/10.1109/TPEL.2012.2196712.

[12] E. Babaei and S. Laali, "A Multilevel Inverter with Reduced Power Switches," *Arabian Journal for Science and Engineering*, vol. 41, no. 9, pp. 3605–3617, Sep. 2016, https://doi.org/10.1007/s13369-016-2217-0.

[13] H. K. Busireddy, M. M. Lokhande, R. R. Karasani, and V. B. Borghate, "A Modified Space Vector PWM Approach for Nine-Level Cascaded H-Bridge Inverter," *Arabian Journal for Science and Engineering*, vol. 44, no. 3, pp. 2131–2149, Mar. 2019, https://doi.org/10.1007/s13369-018-3363-3.

[14] W. Li, X. Zhang, Z. Zhao, G. Zhang, G. Wang, and D. Xu, "Implementation of Five-Level DPWM on Parallel Three-Level Inverters to Reduce Common-Mode Voltage and AC Current Ripples," *IEEE Transactions on Industry Applications*, vol. 56, no. 4, pp. 4017–4027, Jul. 2020, https://doi.org/10.1109/TIA.2020.2991020.

[15] T. Liu, A. Chen, C. Qin, J. Chen, and X. Li, "Double Vector Model Predictive Control to Reduce Common-Mode Voltage Without Weighting Factors for Three-Level Inverters," *IEEE Transactions on Industrial Electronics*, vol. 67, no. 10, pp. 8980–8990, Oct. 2020, https://doi.org/10.1109/TIE.2020.2994876.

[16] M. Jamil, "Carrier-based modulation strategies for a neutral point clamped inverter," *International Journal of Electronics*, vol. 95, no. 12, pp. 1293–1303, Dec. 2008, https://doi.org/10.1080/00207210802524294.

[17] A. Alexander Stonier, "Design and development of high performance solar photovoltaic inverter with advanced modulation techniques to improve power quality," *International Journal of Electronics*, vol. 104, no. 2, pp. 174–189, Feb. 2017, https://doi.org/10.1080/00207217.2016.1196746.

[18] P. S. Kumar and M. Satyanarayana, "Comparative analysis of modulation strategies applied to seven-level diode clamped multi-level inverter fed induction motor drive," in *Conference on Power, Control, Communication and Computational Technologies for Sustainable Growth*, Kurnool, India, Dec. 2015, pp. 231–237, https://doi.org/10.1109/PCCCTSG.2015.7503893.

[19] M. A. Siddiqui, M. N. Anwar, and S. H. Laskar, "Sliding mode controller design for second-order unstable processes with dead-time," *Journal of Electrical Engineering*, vol. 71, no. 4, pp. 237–245, Aug. 2020, https://doi.org/10.2478/jee-2020-0032.

[20] U. Mehta and I. Kaya, "Smith predictor with sliding mode control for processes with large dead times," *Journal of Electrical Engineering*, vol. 68, no. 6, pp. 463–469, Nov. 2017, https://doi.org/10.1515/jee-2017-0081.

[21] V. Q. Nguyen, Q. T. Tran, and H. N. Duong, "Stator-flux-oriented control for threephase induction motors using sliding mode control," *Journal of Electrical Systems*, vol. 16, no. 2, pp. 171–184, 2020.

[22] K. Ullah, J. Guzinski, and A. F. Mirza, "Critical Review on Robust Speed Control Techniques for Permanent Magnet Synchronous Motor (PMSM) Speed Regulation," *Energies*, vol. 15, no. 3, Jan. 2022, Art. no. 1235, https://doi.org/10.3390/en15031235.

[23] T. Abdelwahed, M. Radouane, T. Abderrahim, M. Aboulfatah, and R. Nabila, "Comparative study between fast terminal and second order sliding mode controls applied to a wind energy conversion system," *Indonesian Journal of Electrical Engineering and Computer Science*, vol. 22, no. 2, pp. 765–779, May 2021, https://doi.org/10.11591/ijeecs.v22.i2.

[24] G. Tarchala, "Sliding mode speed control of an induction motor drive using time-varying switching line," *Power Electronics and Drives*, vol. 2, no. 37, pp. 105–120, 2017, https://doi.org/10.5277/PED170109.

[25] I. Eker, "Second-Order Sliding Mode Control with PI Sliding Surface and Experimental Application to an Electromechanical Plant," *Arabian Journal for Science and Engineering*, vol. 37, no. 7, pp. 1969–1986, Oct. 2012, https://doi.org/10.1007/s13369-012-0290-6.

[26] A. Guezmil, H. Berriri, A. Sakly, and M. F. Mimouni, "Sliding Mode-Based Active Fault-Tolerant Control for Induction Machine," *Arabian Journal for Science and Engineering*, vol. 45, no. 3, pp. 1447–1455, Mar. 2020, https://doi.org/10.1007/s13369-019-03982-9.

[27] M. H. N. Razali, J. M. Lazi, Z. Ibrahim, M. H. N. Talib, and F. A. Patakor, "Sliding mode control with observer for permanent magnet synchronous machine drives," *Indonesian Journal of Electrical Engineering and Computer Science*, vol. 25, no. 1, pp. 89–97, Jan. 2022, https://doi.org/10.11591/ijeecs.v25.i1.pp89-97.

[28] V. Q. Vinh and V. T. Ha, "Improved Torque Ripple of Switched Reluctance Motors using Sliding Mode Control for Electric Vehicles," *Engineering, Technology & Applied Science Research*, vol. 13, no. 1, pp. 10140–10144, Feb. 2023, https://doi.org/10.48084/etasr.5559.

[29] J. A. Cortajarena, O. Barambones, P. Alkorta, and J. De Marcos, "Sliding mode control of grid-tied single-phase inverter in a photovoltaic MPPT application," *Solar Energy*, vol. 155, pp. 793–804, Oct. 2017, https://doi.org/10.1016/j.solener.2017.07.029.

[30] N. B. Kumar and V. Urundady, "Sliding Mode Controller with Integral Action for DC-Link Voltage Control of Grid-Integrated Domestic Photovoltaic Systems," *Arabian Journal for Science and Engineering*, vol. 45, no. 8, pp. 6583–6600, Aug. 2020, https://doi.org/10.1007/s13369-020-04531-5.

[31] Z. Afshar, M. M. Zadeh, and S. M. T. Bathaee, "Sliding Mode Control of Grid-connected Inverters Using Inverter Output Current," in *IEEE International Conference on Environment and Electrical Engineering and 2019 IEEE Industrial and Commercial Power Systems Europe (EEEIC / I&CPS Europe)*, Genova, Italy, Jun. 2019, pp. 1–5, https://doi.org/10.1109/EEEIC.2019.8783278.

[32] M. A. G. de Brito, E. H. B. Dourado, L. P. Sampaio, S. A. O. da Silva, and R. C. Garcia, "Sliding Mode Control for Single-Phase Grid-Connected Voltage Source Inverter with L and LCL Filters," *Eng*, vol. 4, no. 1, pp. 301–316, Mar. 2023, https://doi.org/10.3390/eng4010018.

[33] S.-A. Touil, N. Boudjerda, A. Boubakir, and A. Boudouda, "Sliding mode control of a grid-connected photovoltaic source via a three-phase inverter using incremental conductance MPPT," in *5th International Conference on Electrical Engineering - Boumerdes (ICEE-B)*, Boumerdes, Algeria, Oct. 2017, pp. 1–6, https://doi.org/10.1109/ICEE-B.2017.8192220.

[34] X. Zheng, K. Qiu, L. Hou, Z. Liu, and C. Wang, "Sliding-mode control for grid-connected inverter with a passive damped LCL filter," in *13th IEEE Conference on Industrial Electronics and Applications*, Wuhan, China, Jun. 2018, pp. 739–744, https://doi.org/10.1109/ICIEA.2018.8397811.

[35] C. Dang, X. Tong, and W. Song, "Sliding-mode control in dq-frame for a three-phase grid-connected inverter with LCL-filter," *Journal of the Franklin Institute*, vol. 357, no. 15, pp. 10159–10174, Oct. 2020, https://doi.org/10.1016/j.jfranklin.2019.12.022.

[36] S.-J. Yoon, T. V. Nguyen, and K.-H. Kim, "Current control of grid-connected inverter using integral sliding mode control and resonant compensation," *International Journal of Power Electronics and Drive Systems*, vol. 10, no. 2, pp. 1022–1033, Jun. 2019, https://doi.org/10.11591/ijpeds.v10.i2.pp1022-1033.

[37] F. Sebaaly, H. Vahedi, H. Y. Kanaan, N. Moubayed, and K. Al-Haddad, "Sliding Mode Fixed Frequency Current Controller Design for Grid-Connected NPC Inverter," *IEEE Journal of Emerging and Selected Topics in Power Electronics*, vol. 4, no. 4, pp. 1397–1405, Dec. 2016, https://doi.org/10.1109/JESTPE.2016.2586378.

[38] M. A. Rafiq, A. Ulasyar, W. Uddin, H. S. Zad, A. Khattak, and K. Zeb, "Design and Control of a Quasi-Z Source Multilevel Inverter Using a New Reaching Law-Based Sliding Mode Control," *Energies*, vol. 15, no. 21, Jan. 2022, Art. no. 8002, https://doi.org/10.3390/en15218002.

[39] N. V. Quan and M. T. Long, "An improved control method for cascaded multilevel inverters based on sliding mode control technique," *Electrical Engineering*, vol. 105, no. 5, pp. 3293–3306, Oct. 2023, https://doi.org/10.1007/s00202-023-01882-8.

[40] T. Quangtho and N. Vinh Quan, "Reduction of common mode voltage for grid-connected multilevel inverters using fuzzy logic controller," *International Journal of Power Electronics and Drive Systems*, vol. 14, no. 2, pp. 698–707, Jun. 2023, https://doi.org/10.11591/ijpeds.v14.i2.pp698-707.

[41] X. Zhang, L. Sun, K. Zhao, and L. Sun, "Nonlinear Speed Control for PMSM System Using Sliding-Mode Control and Disturbance Compensation Techniques," *IEEE Transactions on Power Electronics*, vol. 28, no. 3, pp. 1358–1365, Mar. 2013, https://doi.org/10.1109/TPEL.2012.2206610.